Open-Loop Subsonic Suction Type Wind Tunnel: Design, Simulation, Build and Test

Kok-Hoe Wong[1,2,*], Weldon Lai[2], Jing-Hong Ng[2], Ahmad Fazlizan[3], Kamaruzzaman Sopian[4], Niranjan Sahoo[5]

[1] Carbon Neutrality Research Group (CNRG), University of Southampton Malaysia, 79100 Iskandar Puteri, Johor, Malaysia
[2] Department of Mechanical Engineering, Faculty of Engineering and Physical Sciences, University of Southampton Malaysia, 79100 Iskandar Puteri, Johor, Malaysia
[3] Solar Energy Research Institute (SERI), The National University of Malaysia, 43600 Bangi, Selangor, Malaysia
[4] Department of Mechanical Engineering, Universiti Teknologi PETRONAS, 32610 Seri Iskandar, Perak, Malaysia
[5] Department of Mechanical Engineering, Indian Institute of Technology Guwahati, Assam 781039, India

ARTICLE INFO	ABSTRACT
  Keywords: 	The technological advancement in drones, unmanned aerial vehicles (UAV), wind turbines, and airfoil research has grown rapidly since last decade. Computational fluid dynamics (CFD) analysis is commonly used to study the airflow around a body. Yet, the wind tunnel is an essential instrument in aerodynamic research; however, a commercial wind tunnel normally comes with a small test section and incurs high investment costs. This paper presents the development of a low-cost subsonic open-loop wind tunnel for research and education purposes. The suction-type wind tunnel is intentionally designed with a large test section of 1 m² and in modular form where each section can be rectified according to the application and for different wind tunnel parameter studies. The detailed design steps, fabrication method, and build of the tunnel are described, along with the flow analysis that has been conducted. Furthermore, a 3D CFD simulation has been performed to simulate the flow condition of the wind tunnel where a good agreement between the simulation and flow measurement is observed. The potential root cause for discrepancy and comparisons with other wind tunnels are discussed. From the preliminary test, wind flow velocity and the turbulence intensity (TI) obtained from the flow measurement are 5.16 m/s and 3.14 % respectively. The TI is less than < 5%, which is considered a medium turbulence case that is good to study the flow around small-scale specimens like micro wind turbines and UAVs.

1. Introduction

Over the past few decades, the wind tunnel has been a significant tool utilized in several green energy and aerodynamics studies such as the study of wind turbines, testing of new wing designs, aerodynamic characteristics, and others [1-3]. Various research and application in engineering employ a wind tunnel in their study. A comprehensive review has been conducted by He *et al.,* on

---

the wind tunnel study for wind turbines [4]. Wind tunnels have also been used for wind turbine [5-8] and wind farm layout optimization (WFLO) studies where Chowdhury *et al.,* study the WFLO using the constrained Particle Swarm Optimization and validated it with a scaled-down wind tunnel study of 3 x 3 array wind turbine models [9]. Segalini *et al.,* performed an experiment on wind farm blockage [10]. In the building sector, a boundary layer wind tunnel is commonly used to simulate the flow around tall buildings and to study the wind load effect of façade, the arrangement of buildings, and their responses [11-16]. Nevertheless, the study of micro air vehicles [17], airfoils [18-19], and automobiles can also be performed in a wind tunnel [20-21].

Despite the CFD technique being widely used [22], wind tunnel testing data still serve as the basis for engineering decision-making. There are several ways to classify wind tunnels which are based on the flow regime, the type of configurations and the type of application. For the flow regime or based on the Mach number, it can be categorized as

    i.   Subsonic (Ma< 0.8)
    ii.   Transonic (0.8 < Ma < 1.2)
    iii.   Supersonic (1.2 < Ma < 5.0)
    iv.   Hypersonic (Ma > 5.0)

While for the configuration or flow circulation of the wind tunnel, basically it is divided into open-circuit and closed-circuit wind tunnels. In addition, it can be sub-classified by three main characteristics, which are the form of the test section (open, half-open, and sealed), the form of the channel of a wind tunnel (blow type, suction type, and circulating type), as well as the existence of flow circulation as shown in Figure 1 [6]. In terms of the application of wind tunnels, some specialized wind tunnels including high enthalpy wind tunnels, atmospheric entry wind tunnels, climatic wind tunnels, shock tubes or blow-down wind tunnels, anechoic wind tunnels, boundary layer wind tunnels, icing wind tunnels, etc. are used for specific applications.

Yokoi [23] also listed favourable advantages of implementing the suction-type wind tunnel. For instance, its rectification part can be composed more compactly compared to the blow type. Apart from that, the temperature of the test section can be assumed to be the same as the surrounding temperature. However, the weakness is that the suction type can be influenced by the fluctuation of the outer air flow. Hence, the test section must become negative pressure relative to the atmospheric pressure. In most wind tunnel experiments today, the actual phenomenon of the flow properties is very difficult to be achieved because of the variation in free stream pressure in the developing zone of the wind tunnel [24]. Therefore, several investigations had been conducted by scientists and researchers around the world to discover ways to improve wind tunnels through computational simulations and experiments.

Duct Type \ Test Section	Open-type	Half-open Type	Sealed Type
Blow			
Suction	Non-practical		
Circulating Blow			
Circulating Suction	Non-practical		
Circulating (Closed Loop)			

Fig. 1. Wind tunnel classifications; the blower is represented by the fan icon, whereas the flow direction and test section are represented by the arrow and "T.S." respectively Duct Type Test Section [23]

Wibowo and Al-Obaidi [2] experimented with an open circuit (Eiffel) wind tunnel, focusing on the quantification of potential sources of experimental errors, to discover solutions to improve the accuracy of measurements. The test section of the tunnel has a cross-sectional area of 0.303 m x 0.303 m and a length of 0.885 m. The contraction ratio of the tunnel is 3:4:1, while the wind speed varied from 3.33 to 38.85 m/s. Four distinct experiments were conducted to investigate the errors under 4 parameters which are the flow rate, the effect of air leakage, test rig, and size of the model in the wind tunnel. The velocity distribution along the centreline of the test section was measured at three different locations. The experimental results showed that the contribution of error percentages was 0.65% (flow rate), 1.23% (effect of air leakage), 24.87% (test rig), and 20.18% (size of the model) respectively. Motin and Ali [24] designed and constructed an open circuit wind tunnel that consisted of a 1.22 m long test section with a cross-sectional area of 0.3 m x 0.3 m, operating at a maximum air speed of 22 m/s. The fan with its discharge unit was separated from the entry unit by using a damper so that the vibration could be minimized. The velocity profiles were determined at several points in the streamwise direction, with the pitot-static tube being connected to both the micromanometer and pressure transducer in parallel. It was determined that the free stream velocity is not constant throughout the test section. Instead, it increases slowly in the downstream direction. This is due to

the development of the boundary layer along the walls of the test section, which then reduces the cross-sectional area for the flow, causing the acceleration of the free stream flow. Nader *et al.,* [25] experimented to measure the velocity profile and turbulence intensity in a wind tunnel with a contraction ratio of 16, and a test section with a length of 2 m and cross-sectional area of 0.5 m x 0.5 m, which was divided into 49 subsections with a 7 x 7 configuration. The calibrations of the velocity sensors and constant temperature hot-wire anemometer were performed before the experiment. It was shown that the average velocity variation is within ±0.2% of the centre velocity (above ±0.5% for extreme cases), while the mean turbulence intensity for flow velocity of 2.5 to 20 m/s was below 0.4%. Pedro *et al.,* [26] built a wind tunnel with a longer test section compared to other papers. The test section has a cross-sectional area of 0.8 m x 0.6 m, with a length of 5 m. Two screens were added to the effuser of the wind tunnel to further reduce the velocity fluctuation in the test section. The velocity and turbulence profiles in the test section were measured under wind speeds of 5, 15, and 30 m/s in the planes located at 1.8, 2.6 and 3.4 m from the flow inlet using a constant temperature hot-wire anemometer. The experimental results showed that the turbulence intensity values were the highest in the first point of measurement near the walls in both the Y- and Z- axes. For the velocity of 15 m/s, the turbulence intensity was about 5% near the walls, confirming the formation of the boundary layer. Overall, the velocity variations in the free stream inside the test section were less than 1% and turbulence intensity was less than 4% for all the conditions evaluated. It was also pointed out that the contraction nozzles had successfully reduced the turbulence intensity from 6.5% (original configuration) to 4%. Thimmegowda and Krishnan [27] have tested the flow quality of an open-loop low-speed wind tunnel both computationally and experimentally, where the ANSYS CFX software was implemented for the computational simulation of flow. The wind tunnel was designed to have a contraction ratio of 9 and a 0.6 m x 0.6 m test section with a length of 2 m. The design parameters considered included boundary layer separation, controlled airflow quality, turbulence intensity, a streamlined flow, cost-effectiveness, and design ease at a Mach number of 0.15. The design has successfully maintained the smooth quality of the flow with no boundary layer thickening process at the test chamber. From the experiment, it was determined that the flow velocity increases as it moves through the effuser and is highest when it reaches the test section, after which it will remain constant throughout the test section and subsequently decreases in the diffuser. The uniformity of the flow at the test section centreline remains constant along the length of the tunnel with zero-degree flow angularity, which agrees well with the simulation results.

It is always an issue that for a small test section wind tunnel, the testing object is limited to scaled-down models or for 2D model study purposes, e.g., airfoil profile. For the case of wind turbine study, the scaled-down model would limit the actual performance of the turbine due to high solidity where vortex shedding, and blade wake interaction effect are significant. While in the drone or UAV model study, an actual size model is normally used. The blockage ratio effect of a small test section can cause serious distortion of the test data [28]. The purpose of this work is to design and build a low-cost wind tunnel with a large test section that is suitable for micro wind turbines, UAVs, drones, etc. testing purposes. This paper will provide a guide to wind tunnel development, fabrication, flow quality measurement, and CFD simulation. The flow quality in the test section of the wind tunnel is determined by measuring the turbulence intensity, flow velocity, and flow uniformity. The full-scale wind tunnel will also be analyzed numerically to validate the results acquired from the experiment. From the literature, most tunnels that obtained a high wind velocity with a small test section are limited to scaled-down models. In addition, if the test section is more than 1 m^2, it tends to be a closed loop large-scaled wind tunnel which incurs a high investment cost and occupies a large space. The aim of the research is to build a large test section, low-cost open-loop wind tunnel with an acceptable range of wind speed. Furthermore, the wind tunnel is designed in a way that it is portable

and modular, where modification can be adopted by replacing the effuser, test section, or diffuser for the study of different wind flow conditions and tunnel parameters.

Followed by this section, the design aspects of the tunnel are reported in Section 2. Section 3 reveals the fabrication, assembly, and flow test, while the CFD simulation of the tunnel is explained in Section 4. Results of the flow measurement and CFD as well as relevant discussion are reported in Section 5. Lastly, the conclusion and future works are included in Section 6.

2. Design and Modelling of Wind Tunnel

In this study, the open-loop suction-type wind tunnel comprises 3 main sections: effuser or contraction section, test section, and diffuser. A few design specifications are pre-defined in the design process which is constrained by the room size, standard material size, components, and manufacturing processes. The size of the test section is set as 1 m x 1 m, which is sufficiently large to fit a micro wind turbine, drone, and scaled-down UAV models. The temperature control of the tunnel is neglected for an open-loop wind tunnel because the ambient air temperature is used as the operating temperature. Despite the temperature of the tunnel not being controlled by the tunnel, the room is under air conditional control. Table 1 below shows the specification of the wind tunnel.

Table 1
Wind tunnel design specifications

Specification	Size
Total length of tunnel	6.85 m
Contraction entry size	2.3 m x 2.3 m
Contraction exit size	1 m x 1 m
Contraction area ratio	5.29
Flow straightener size	1 m (W) x 1 m (H) x 0.265 m (L)
Flow straightener cell size	35 mm x 35 mm
Flow straightener porosity	0.85
Screen porosity	0.88
Test section size	1 m (W) x 1 m (H) x 2 m (L)
Diffuser length	1.573 m
Diffuser entry size	1 m x 1 m
Diffuser inclination angle	4°

2.1 Design Specification
2.1.1 Effuser or contraction section

The effuser or contraction section serves as the inlet of the airflow. It is a converging duct placed upstream of the test section to accelerate the air before the test section. The flow condition in the test section is highly affected by the effuser in which the contraction ratio (a_c) is one of the main parameters as shown in Eq. (1) [29]. Usually, a_c is designed between 4 to 20 for a subsonic wind tunnel [29]. In this work, a_c is set as 5.29 with an entry size of 2.3 m x 2.3 m; this size is selected due to the limitation of standard sheet metal size available in the market, and the size of the room while maximizing the a_c ratio with the test section size as shown in Figure 2.

$$a_c = \frac{Cross-section\ area\ of\ the\ entry}{Cross-section\ area\ of\ the\ exit} \tag{1}$$

Many studies show that the shape of the contraction cone leads to a smooth transition of flow from the entry to the test section where the polynomial curve is applied [30-31]. In this study, for the sake of simplifying the manufacturing process of sheet metal forming, flat panels are used in the effuser.
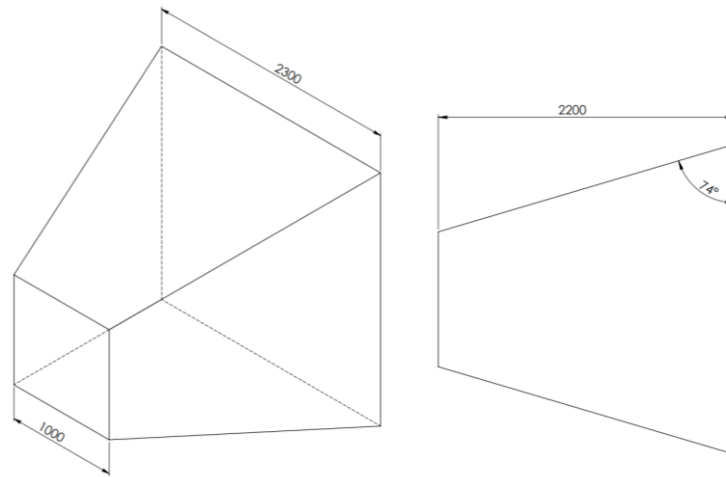
Fig. 2. Design parameters of the effuser isometric view and side view

The second function of the effuser with the settling chamber is to produce a uni-direction and uniform airflow by reducing the swirl and eddies flow. This can be done by using a flow straightener/ honeycomb and screens. As shown in Figure 2, the screen is located at the entry of the contraction cone that covers an area of 2300 mm x 2300 mm, while the exit accommodates the flow straightener. The screen is made of a metal wire mesh of 13 mm x 13 mm size with a wire diameter of 0.8 mm that is used to break up large eddies into smaller eddies that decay faster. With Eq. (2), the screen porosity, B_s calculated is 0.88 [29]. where d is the diameter of wire, and s is the spacing between wires.

$$B_S = (1 - \frac{d}{s})^2 \tag{2}$$

The flow straightener or honeycomb allows airflow in one direction that is parallel to the tunnel, hence, the cross-flow velocities will not cause swirl flow in the tunnel. With the cell length to cell hydraulic diameter ratio between 5-10, it can restrain the boundary layer thickness. Generally, there are 3 different geometries recommended – circular, square, and hexagon. Typically, the hexagon flow straightener is used because it best suppresses the lateral component of turbulence flow with minimum pressure loss [29], however, a square flow straightener is employed due to the ease of the manufacturing process. Although flow uniformity can be achieved by the flow straightener, nevertheless, the high-pressure drop could be induced with wrong sizing.

Flow straightener with 676 cells (26 cells x 26 cells) of each cell 35 mm x 35 mm covers an area of 1 m x 1 m and a length of 250 mm is made of corrugated plastic board. As shown in Eq. (3) [31], the honeycomb porosity, B_h, is the ratio between airflow area to the total area obtained in this work is 85.56% which is more than the recommended value of 80% [29,31]. The length to hydraulic diameter ratio (Eq. (4)) should be kept between 6-8 times the cell dimension [31,32]. In this design, a ratio of approximately 7 is obtained.

$$B_h = \frac{A flow}{A total} \tag{3}$$

$$6 \leq \frac{L, honeycomb}{Dh, honeycomb} \leq 8 \tag{4}$$

2.1.2 Test section

In this design, the test section is set as 1 m (W) x 1 m (H) x 2 m (L) since one of the objectives of the tunnel is to have a large test section to fit the micro wind turbines, drones, or UAVs with a reasonable blockage ratio. The tunnel blockage ratio is the ratio of frontal area of the test model to the wind tunnel cross-sectional area. According to [33], a blockage ratio below 10% is acceptable for the wind tunnel test. If the ratio is higher than the acceptable range, a blockage correction needs to be taken into account [34] or it will cause serious distortion in the test data [28]. The test section is designed with transparent walls to observe the test unit during testing. The airflow velocity is desired to achieve between 5-10 m/s. As the tunnel design comprises 3 modular sections, a higher wind speed can be obtained with a smaller test section or a more powerful driving fan. According to [31], the test section length should be around 0.5-3 times the hydraulic diameter (D_H) Eq. (5) to achieve uniform airflow [35]. where A is the cross-sectional area, and P is the perimeter. In this case, the D_H is 1, where the length-to-D_H ratio is 2.

$$D_H = \frac{4A}{P} \tag{5}$$

2.1.3 Diffuser and suction fan

The diffuser is the section between the test section and the fan with the main function to allow airflow to expand when exiting the test section, hence reducing the dynamic pressure and recovering the static pressure to increase efficiency. The area ratio should be less than 2.5 and the angle between 5-10 °, where a larger angle will initiate the flow separation of the boundary layer [36]. In this diffuser design, the angle is set as 4° with the consideration of the fan size and the diffuser length as shown in Figure 3.

The driving unit serves to maintain the tunnel at the desired constant speed while compensating the pressure drop losses. For the driving unit selection, it is based on the required flow speed of the test section and the pressure drop in the wind tunnel. Since the test section area, S_{TS} is pre-set as 1 m x 1 m to keep a large cross-sectional area, while the target wind speed, V is set at least 5 m/s; the flow rate, Q is 18000 m³/hr without considering the pressure drop and losses. As shown in Eq. (6) to Eq. (8), the power required can be calculated [37].

$$\Delta p = \frac{1}{2} \rho V^2 \varsigma \tag{6}$$

$$Q = V S_{Ts} \tag{7}$$

$$P = \Delta p \frac{Q}{\eta} \tag{8}$$

where Δp is the pressure increment, Q is the volume flow rate, P is the power required, ς is the total pressure loss coefficient, ρ is the air density, and η is the fan efficiency.

The driving fan used is a commercial fan in a rectangular casing in 1220 mm x 1220 mm size. The diameter of the blade is 1100 mm with an airflow of 38000 m³/hr from the datasheet provided by the supplier. The belt-driven propeller fan comprises 6 blades that evenly surround the hub at 60° apart from each other. The blades are made of stainless-steel sheet metal forming with 200 mm width and 455 mm length which can rotate at 450 rpm. Low noise of about 70 dB is generated by the fan. The voltage supply is 50 Hz, 240 V, and single phase with a 0.75 kW motor. There is no speed control for the driving fan, hence only one rotational speed for the tunnel is examined.

The theoretical flow speed obtained without considering losses is 10.5 m/s. However, after measurement, the actual volumetric flow rate of the fan obtained is only approximately 21705 m³/hr. Figure 4 shows the CAD model of the full tunnel assembly.
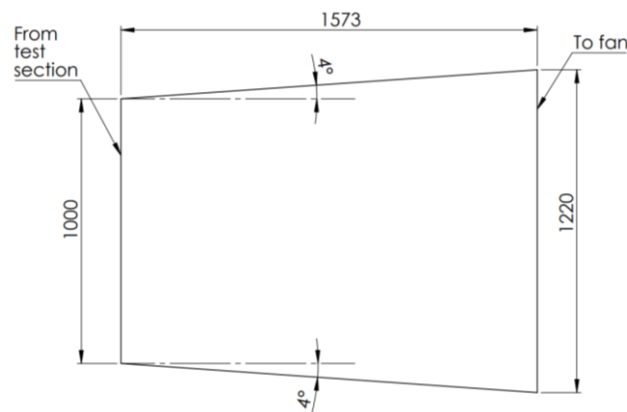
Fig. 3. Design parameters of the diffuser
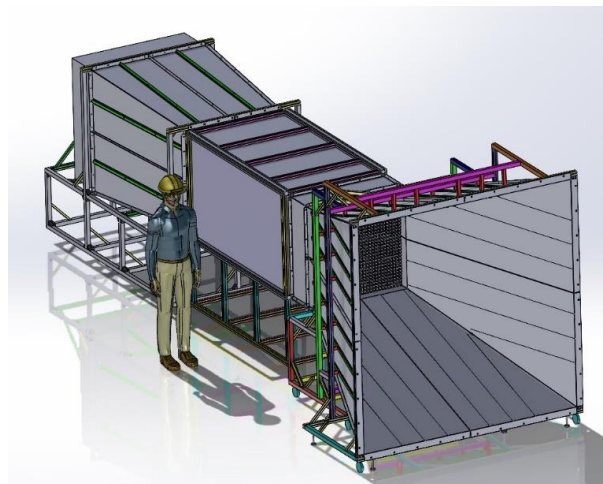
Fig. 4. CAD model of the wind tunnel design

3. Fabrication, Assembly and Flow Test
3.1 Fabrication and Assembly

The galvanized carbon steel sheet metal of 1.5 mm thickness is used to fabricate the effuser and diffuser panels. The selection of thickness is to ensure minimum vibration created on the panel during testing, while the panels are not overly heavy that require more supporting structure. Each side of the effuser and diffuser consists of 2 panels respectively due to the standard material size of 8 ft x 4 ft available in the market. In total, 8 panels are used to construct the effuser and diffuser respectively. The panels are fastened together, and the connection gap is sealed with tape. Reinforced beams are

welded to the panel to increase the strength and provide the mounting point for the panel during assembly to the supporting frame. Figure 5 shows the fabrication of the panel in the factory. White powder coating is used to prevent the corrosion of metal and to ensure a smooth surface of the panel to reduce flow separation and ensure small boundary layer thickness. For the test section, an 8 mm thick acrylic panel is selected due to its transparent property, strength, and lighter weight compared to glass.
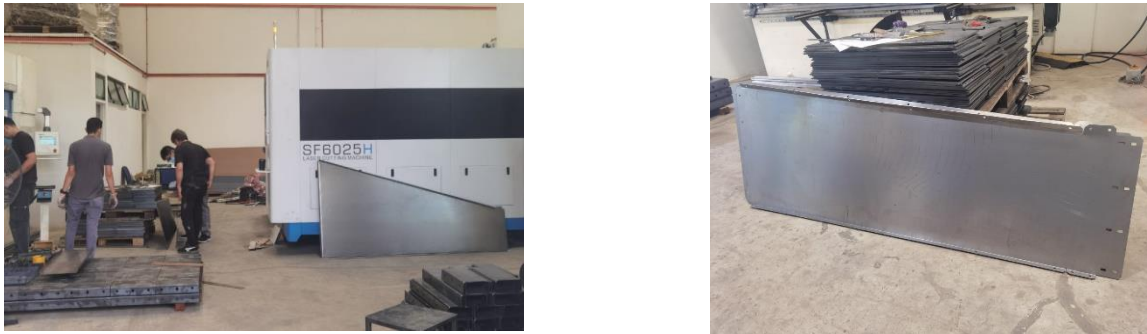
Fig. 5. Sheet metal cutting, bending, and welding processes for the effuse, settling chamber, and diffuser panels

For every section, the sheet metals and the acrylic panels are assembled with the supporting frame, which is the standard 40 mm x 40 mm extruded aluminium conveyor available in the market. Each of the support frames was cut into sizes and assembled with angle brackets at every joint. To further reinforce the structure strength, a metal triangle frame is added for every major connection with long support frames. For the effuser, due to its heavy weight, additional support structures were used to mount the panel to the supporting frame as shown in Figures 6-8. To prevent air leakage, 10 mm foam was used to seal the gap between the 3 main sections, and all gaps between panels is sealed with thin film tape.

(a)

(b)

(c)
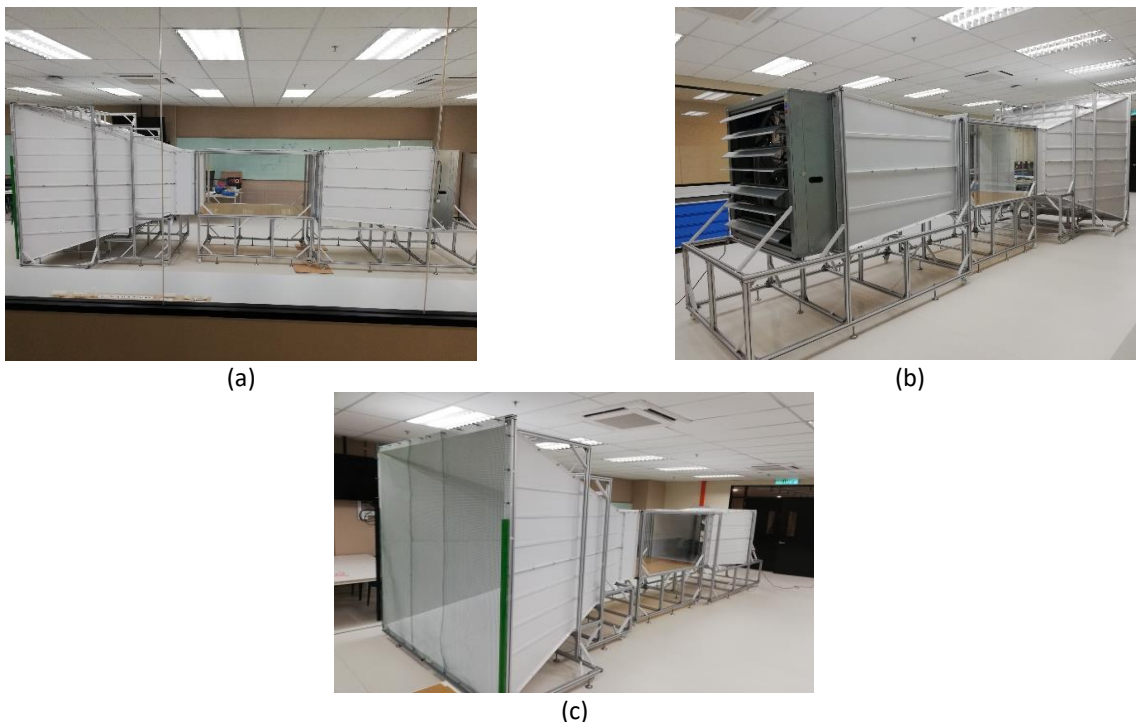
Fig. 6. Complete assembly of the wind tunnel (a) side view (b) back corner view (c) front corner view

(a)   (b)
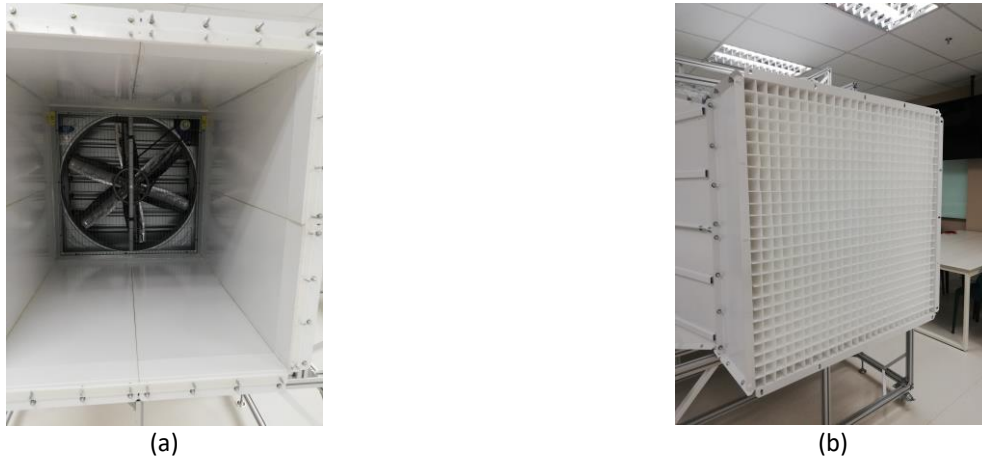
Fig. 7. (a) The diffuser and fan (view from the diffuser inlet) (b) The flow honeycomb section

(a)   (b)

Fig. 8. (a) The modular form of the wind tunnel that parks at the corner of the lab for space saving (b) Assembly work of the tunnel

3.2 Flow Measurement

As shown in Figure 9, the flow velocity in the test section was measured by using a hot wire anemometer. The hot wire anemometer is calibrated with an accuracy of ±5% of the measurement. In total, 9 x 9 wind velocity points are captured in the middle of the test section with every 100 mm spacing interval to cover the 1 m x 1 m test section area. For every point, the sample was recorded every 2 s, and for 1 minute equivalent to 30 data was captured. Detailed flow data are reported in Section 4.
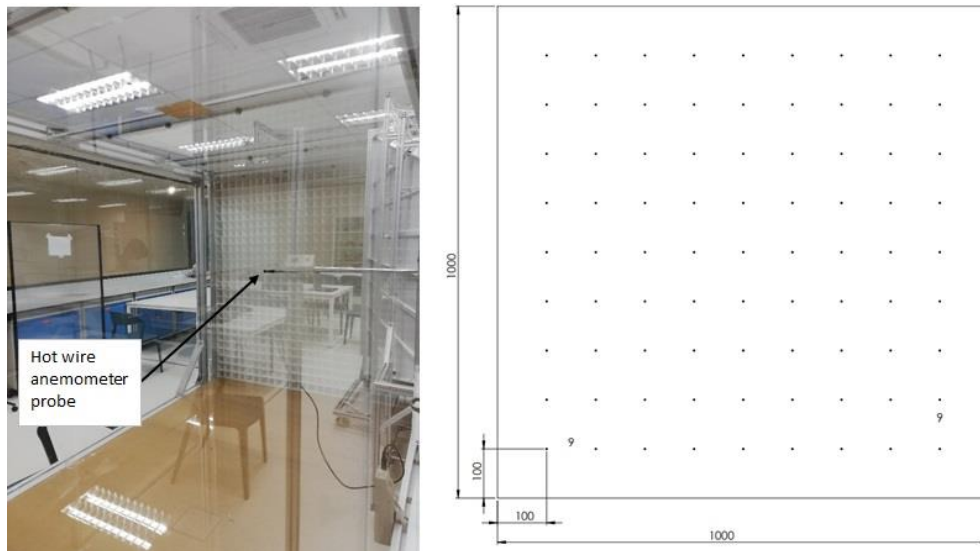
Fig. 9. Velocity measurement of the wind flow using a hot wire anemometer in the wind tunnel

3.3 Bill of Materials

This paper aims to develop a low-cost wind tunnel with a large test section. The cost incurred in the construction of the tunnel is shown in Table 2. The cost is estimated based on a conversion rate of Ringgit Malaysia to US dollar of 1 USD = 4.2 RM. In total, the tunnel incurs about USD 4423. Compared to the million-dollar large-scale closed-loop commercial wind tunnel which usually provides high speeds and large test sections, the cost incurred in this study is relatively low.

Table 2
Bill of Materials

Part/ Component	Material	Quantity	Total Cost (USD)
Effuser panel	Mild steel sheet (1.5 mm thickness)	8	1000
Test section panel	Acrylic sheet (8 mm thickness)	4	733
Diffuser panel	Mild steel sheet (1.0 mm thickness)	8	491
Support bracket	Mild steel sheet (1.0 mm thickness)	64	188
Fan and motor	6 bladed fan, Belt drive, 0.75 kW, 140 rpm, single phase, 50 Hz	1	385
Honeycomb/ Flow straightener	Plastic sheet (3 mm thickness)	35	73
Screen	PVC coated wire mesh	24 m	17
Structure frame	Aluminum conveyor	24 pcs (12 ft length)	920
Frame triangle joint	Aluminum cast	250	61
Wheel	5-inch diameter	14	56
Stand	M10 shaft stand	24	75
Fastener (Bolts, nuts, spring washers, washers)	Steel	bulk	67
Anemometer	Hot wire type	1	357

4. CFD Simulation

4.1 CFD Modelling and Setting

A 3D CFD steady-state simulation was performed to simulate the flow inside the tunnel using the Ansys Fluent software [38]. The tunnel geometry is modelled by the DesignModeler in Ansys. The boundary conditions were set as shown in Figure 10. All 3 sections were modelled in the same geometry where it is assumed that there is no air leakage between the connection of sections. The honeycomb, top, bottom, and side boundaries were set as walls. The entry and the outlet of the tunnel were set as velocity inlet and pressure outlet respectively. The velocity inlet is calculated based on the volumetric flow rate given by the exhaust fan to the area of the entry equal to 1.14 m/s with the actual fan's volumetric flow rate, while the pressure outlet is the same as the atmospheric pressure. Air with the default properties of 1.225 kg/m³ is used as the fluid. The *k-ω SST* turbulence model that is widely used in engineering applications is adopted for the simulation. The semi-Implicit Method for Pressure Linked equation (SIMPLE) algorithm is applied to solve the Navier-Stokes equation with the spatial discretization set as second order for pressure, momentum, turbulent kinetic energy, and specific dissipation rate to obtain higher accuracy.
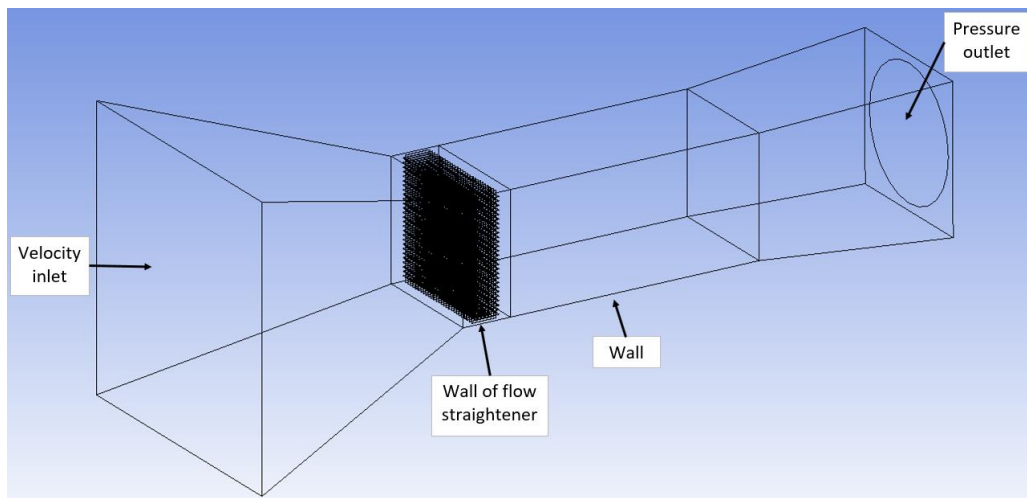
Fig. 10. Geometry and boundary conditions

4.2 Mesh Dependency Test

A mesh dependency test was performed to validate the simulation. Six different mesh sizes with its corresponding number of cells are shown in Table 3 for the domain were investigated.

Table 3
Mesh dependency test

Mesh size (mm)	Number of cells
20	12,063,976
30	3,916,923
40	1,827,553
50	1,035,025
100	214,810
200	80,168

As shown in Figure 11, the mesh domains for fine to coarse mesh size of 20mm, 50 mm and 100 mm. The cell size near the wall boundaries is refined by an inflation layer that gradually increases (Figure 11.d). The first cell height is set to 0.5 mm with a growth rate of 1.2 and 15 layers to ensure a Y+ value of approximately 1 is obtained. The wall cell size is set as 3 mm. From the result of the simulation, there is no significant difference in the flow velocity with the change in mesh size (< 1%), hence, a size of 30 mm for the domain is adopted as shown in Figure 12.
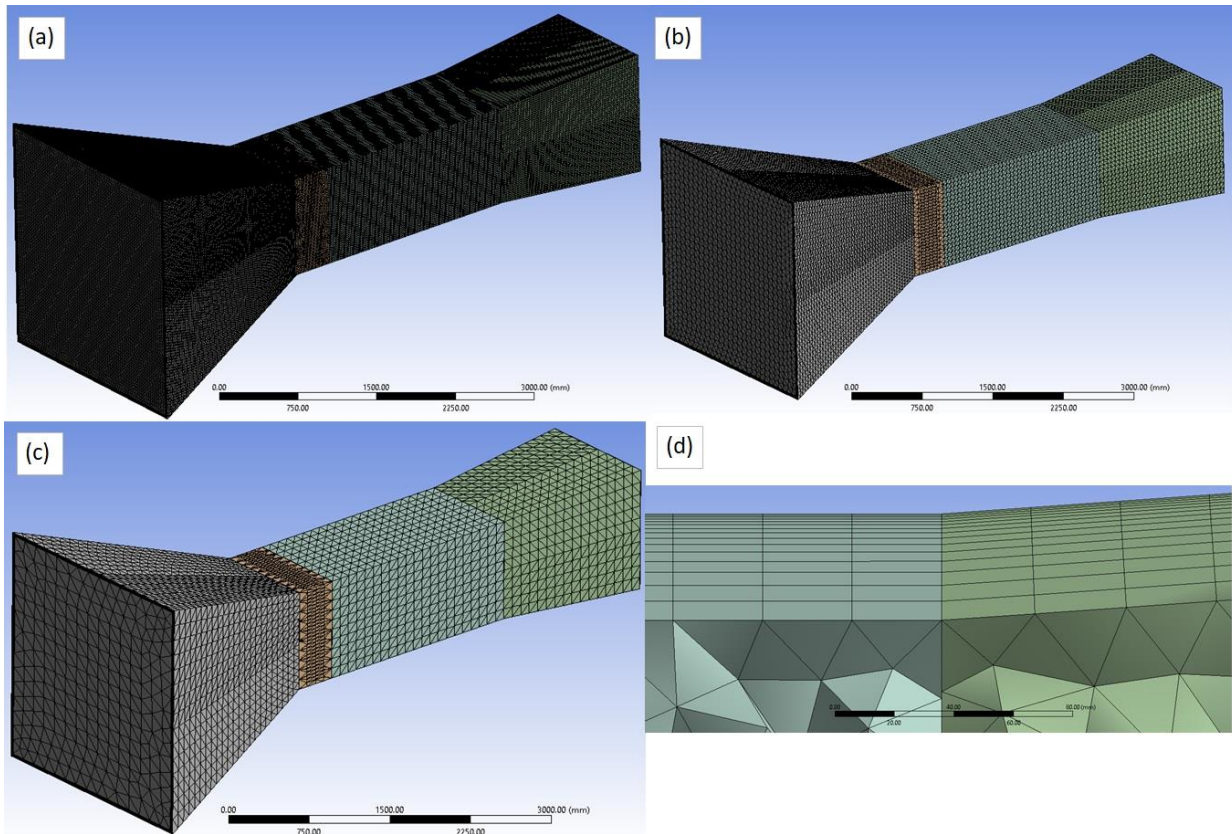
Fig. 11. Mesh size for various mesh sizes (a) 20, (b) 50 and (c) 100 as well as the detailed view of the mesh inflation near the boundary
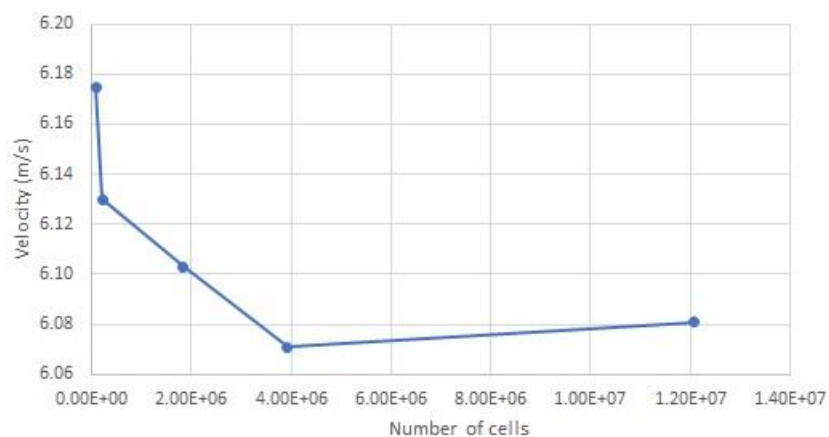
Fig. 12. Mesh independency study- flow velocity against the number of cells of the mid-point

5. Results and Discussions

5.1 Flow Measurement Data

The turbulence intensity is an important parameter to determine the flow condition in a wind tunnel. It represents the deviation from the mean velocity due to the perturbation components of velocities along x-, y-, and z- coordinate directions as shown in Eq. (9) [31]. Where $\overline{U}$ is the mean velocity; u, v, and w are the component velocities. In this tunnel, the x- direction perturbation velocity alone is used to define the turbulence intensity with the Eq. (10) as shown below [31]

$$I_t = \frac{1}{\overline{U}} \sqrt{\frac{1}{3}\left(\overline{u'^2} + \overline{v'^2} + \overline{w'^2}\right)} \tag{9}$$

$$I_t = \frac{\sqrt{\overline{u'^2}}}{\overline{U}} \tag{10}$$

A good flow-quality wind tunnel should achieve flow uniformity and turbulence intensity of 0.5-2%. Table 4 shows the average wind velocity measurement for the middle plane of the test section. From the flow measurement, the average velocity obtained is approximately 5.61 m/s with a maximum wind velocity of 6.01 m/s and minimum velocity of 4.93 m/s among the 81 measuring points, which is corresponding to +0.39 m/s and -0.69 m/s. The turbulence intensity calculated based on Eq. (4) is 3.14%. This is considered a medium turbulence intensity, slightly higher than the target of 2%. The flow measurement was also taken at 25% of the test section inlet, where the data is shown in Table 5. It is found that the average wind velocity is slightly lower at about 5.51 m/s with the maximum and minimum velocities of 5.95 m/s and 5.26 m/s which is about 0.44 m/s and -0.25 m/s difference from the average wind velocity. The turbulence intensity is 2.49%. From the data, it shows that closer to the honeycomb, the turbulence intensity and the wind velocity are slightly lower, and the wind nature is preserved between the quarter to mid-plane of the test section.

For future study, the size of the flow straightener can be further improved to obtain lower turbulence intensity, meanwhile, more screens with different mesh sizes can be included to improve the flow condition. This can be done with the modular design of the tunnel where one more section can be added before the test section in the future. The average flow speed (5.61 m/s) obtained from the flow measurement has a large discrepancy compared to the calculated wind velocity of 10.5 m/s. This is because the fan does not supply a sufficient flow rate as stated in the datasheet (38000 m^3/hr); where the actual flow rate measured from the outlet of the fan only obtained an average of 21705 m^3/hr. In addition, the losses from the flow straightener and minor air leakage were not taken into consideration.

In the design of the tunnel, the test section is made of acrylic, while the effuser and diffuser sheet metal panels are powder-coated to ensure a smooth surface roughness that will reduce the boundary layer thickness. The boundary layer thickness was not measured during the test. However, from the data shown in Table 4, the first measurement point is 10 cm away from the wall, where the flow obtained is considerably uniform. Hence, it shows that the boundary layer is less than 10 cm.

Table 4
Wind speed of the test section in m/s (50% of the test section length)

Location	1	2	3	4	5	6	7	8	9
A	5.32	5.45	5.52	5.58	5.55	5.73	5.71	5.99	5.84
B	4.93	5.71	5.58	5.81	5.61	5.71	5.62	5.65	5.68
C	5.52	5.51	5.44	5.66	5.58	5.6	5.7	5.9	5.79
D	5.13	5.63	5.52	5.26	5.52	5.78	5.84	5.67	5.53
E	5.42	5.64	5.62	5.71	5.7	5.39	5.29	5.46	5.61
F	5.19	5.74	5.6	5.43	5.54	5.38	5.39	5.65	5.77
G	5.43	5.84	6.01	5.77	5.98	5.84	5.73	5.84	5.78
H	5.48	5.88	5.81	5.81	5.76	5.56	5.71	5.65	5.46
I	5.62	5.84	5.7	5.72	5.29	5.53	5.68	5.65	5.56

Table 5
Wind speed of the quarter section from the test section inlet in m/s
(25% of the test section length)

Location	1	2	3	4	5	6	7	8	9
A	5.33	5.39	5.45	5.46	5.58	5.5	5.57	5.6	5.33
B	5.68	5.57	5.6	5.86	5.45	5.5	5.61	5.81	5.26
C	5.38	5.34	5.51	5.32	5.59	5.33	5.52	5.74	5.39
D	5.49	5.69	5.47	5.28	5.45	5.63	5.53	5.7	5.32
E	5.31	5.28	5.71	5.36	5.48	5.41	5.35	5.39	5.37
F	5.58	5.59	5.53	5.36	5.5	5.3	5.63	5.7	5.53
G	5.49	5.95	5.48	5.56	5.48	5.58	5.42	5.65	5.45
H	5.59	5.62	5.4	5.6	5.44	5.46	5.48	5.4	5.36
I	5.87	5.75	5.52	5.27	5.75	5.68	5.65	5.41	5.51

5.2 CFD Simulation Results

From the simulation, 9 points along the middle of the test section are observed horizontally and vertically. Figure 13 shows the velocity contour of airflow in the tunnel in two perpendicular planes and a side view. The flow is quite uniform along the plane. Figure 14 records the simulated velocity and compares it to the experimental result. It shows that the wind flow is accelerated in the contraction cone, and a uniform wind condition is obtained after passing through the flow straightener. The wind velocity obtained from the simulation is about 6 m/s at the centre of the test section. Overall, the simulation overestimates the flow velocity compared to the experiment of about less than 1 m/s. This might be due to one domain being modelled and simulated without an air gap between the sections and the velocity inlet is calculated based on the volumetric flow rate.
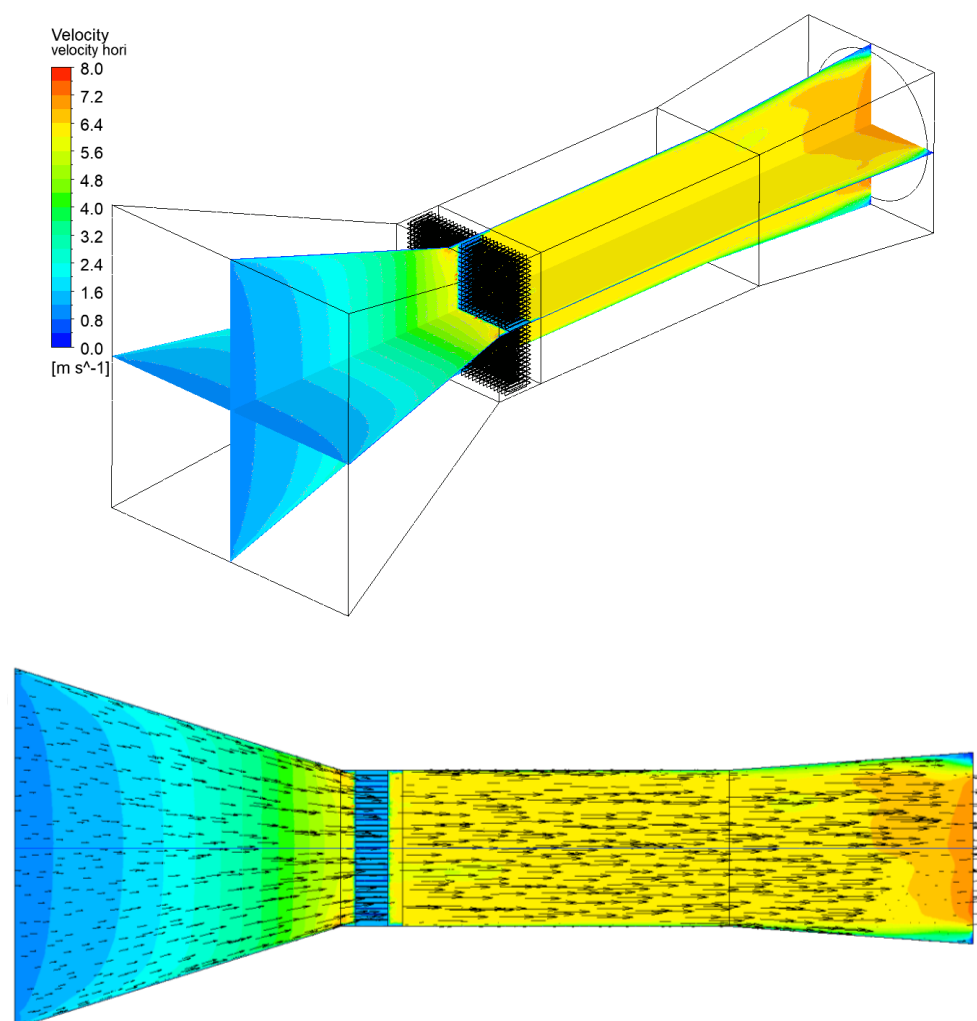
Fig. 13. Velocity contour and velocity vector of the wind tunnel (Isometric and side views)

5.2 CFD Simulation Versus Experimental Data

Figure 14 shows the difference between the CFD simulation and the experiment for 9 measuring points located vertically and horizontally along the middle plane respectively, where point 1 is from the top of the vertical plane and the left of the horizontal plane. It can be observed that the trend follows closely between the simulation and experiment, with the lowest and largest discrepancy happening at point 7 horizontally and point 7 vertically which is about 0.98% and 12.4%. This discrepancy is likely caused by losses occurring in the wind tunnel as the inlet velocity set was based on the assumption that losses or pressure drops were not to be considered. The calculated wind speed according to the volumetric flow rate of the fan is approximately 6.03 m/s without considering the pressure drop at each section of the tunnel (especially the honeycomb and screen sections). As abovementioned, the simulation modelled the tunnel as a body, whereas the actual wind tunnel has some air leaks between the section and metal panels. The inefficiency of the drive unit, skin friction, separation, and loss of kinetic energy at the diffuser exit also contributed to the discrepancy
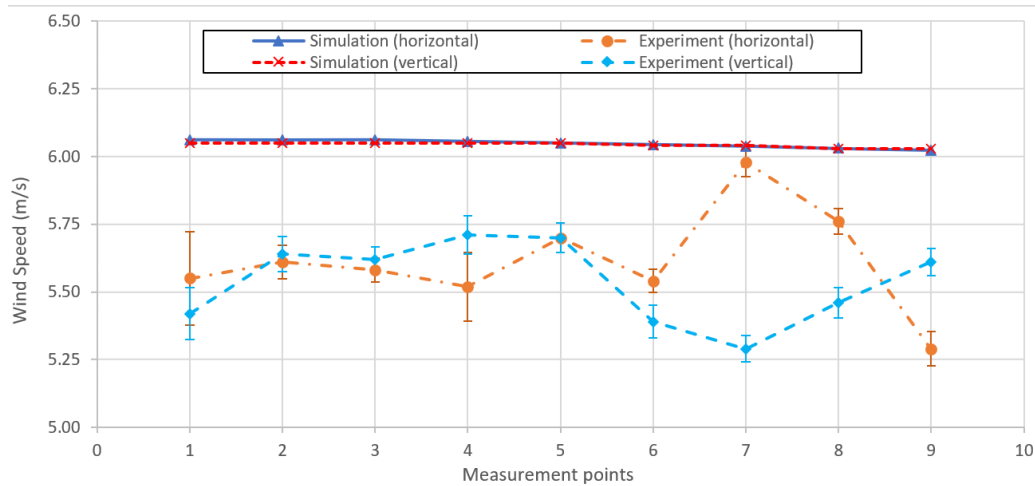
Fig. 14. Comparison between CFD and experimental results with one standard deviation error bar

A comparison between tunnel types has been made and is shown in Table 6. The table demonstrates that the current tunnel design in terms of the test section, flow condition and cost incurred, matched the aim of obtaining a large test section with acceptable wind speed and turbulence intensity while maintaining a low cost. Nevertheless, the main trade-off for a large test section with the same driving unit is obtaining a lower speed.

Table 6
Comparison of small-scale open-loop wind tunnels for research and education purposes

Source	Tunnel type	Test section area (m x m)	Wind speed (m/s)	Experimental turbulence intensity (%)	Driving unit power (kW)	Cost (USD)
Current research	Suction-type	1 x 1	5.6	3	0.75	4423
Ismail et *al.,* [39]	Suction-type	0.75 x 0.75	0-16	0.749	5.5	4534
Chen *et al.,* [40]	Suction-type	1.3x1.3	25	< 1	44.7	-
Mauro *et al.,* [31]	Suction-type	0.005x0.005	6.5	1	0.029	-
Menezes [32]	Blow-type	0.6x0.6	25	-	38880 m^3/hr (flow rate)	9835

Since the design of this tunnel is portable and modular, various wind tunnel parameters can be investigated in the future with low costs incurred. This includes the shape of the effuser, length of the test section, effects of size and number of screens, shape of the diffuser and honeycomb, and replacing a single fan with multiple fans.

The wind speed obtained from the current study achieved 5.61 m/s. As the driving unit is the main component that directly affects the wind speed, changing a large power motor and fan is in planning now for future improvement of the tunnel to achieve a wider overage of wind speed. In addition, a speed control system will be employed to enable the variable speed adjustment. As abovementioned, the fan is square in shape which limits the diffuser size which may reduce ideal flow conditions due to flow separation at the corner. For future planning, a smooth transition diffuser from square to circular will be deployed and the comparison will be studied. The effect of boundary

layer thickness and the flow condition in different lateral distances of the test section will also be considered.

6. Conclusion

A low-cost subsonic wind turbine has been developed in this study. The detailed design procedure, fabrication, and construction of a suction-type tunnel have been reported. This study aims to design a tunnel with a large test section for the actual size model of micro wind turbines, UAVs, drones, and others for research purposes. In addition, unlike a large-scale commercial tunnel, this tunnel is portable and of a modular design where each section can be rectified for different tunnel and components' parameter studies including the screen, size of honey, and type of driving unit. A commercial fan is employed as the driving fan while other parts are designed and fabricated. From the preliminary stage, the average wind velocity measured by a hot wire anemometer for 81 points of the test section plane obtained is 5.61 m/s with a turbulence intensity of 3.14%. In addition, CFD simulation has been performed to visualize the flow condition in the tunnel where a similar flow trend is obtained. The total cost incurred in the construction of this tunnel is about USD 4423. However, due to the large section with the size constraint of the driving unit and the overall tunnel size ratio, the main trade-off is the incurred low wind flow. Since limited wind speed is obtained due to the fixed driving unit, a more powerful driving unit is required for future studies to achieve a higher flow speed. The effects of the mesh size in the flow straightener and the number of screens can be investigated to obtain a better flow condition. Furthermore, a validation test of the tunnel with a specimen such as air foil or a cube that connects to pressure taps will be conducted in the near future.

References

[1] Aboelezz, Ahmed, Yunes Elqudsi, Mostafa Hassanalian, and Ahmed Desoki. "Wind tunnel calibration, corrections and experimental validation for fixed-wing micro air vehicles measurements." *Aviation* 23, no. 4 (2019): 104-113. https://doi.org/10.3846/aviation.2019.11975

[2] Wibowo, Hutomo., Sh. Mahdi Al-Obaidi, Abdulkareem. "Improving the accuracy of Taylor's wind tunnel measurements." *International Engineering Research Conference (8th eureca)* (2017): 322-341.

[3] Jang, Hyeonmu, Yechan Hwang, Insu Paek, and Seungryul Lim. "Performance evaluation and validation of H-darrieus small vertical axis wind turbine." *International Journal of Precision Engineering and Manufacturing-Green Technology* (2021): 1-11. https://doi.org/10.1007/s40684-021-00316-9

[4] He, Ruiyang, Haiying Sun, Xiaoxia Gao, and Hongxing Yang. "Wind tunnel tests for wind turbines: A state-of-the-art review." *Renewable and Sustainable Energy Reviews* 166 (2022): 112675. https://doi.org/10.1016/j.rser.2022.112675

[5] Sewucipto, Sanjaya, and Triyogi Yuwono. "The Influence of Upstream Installation of D-53 Type Cylinder on the Performance of Savonius Turbine." *Journal of Advanced Research in Experimental Fluid Mechanics and Heat Transfer* 3, no. 1 (2021): 36-47.

[6] Zakaria, Ahmad, and Mohd Shahrul Nizam Ibrahim. "Velocity Pattern Analysis of Multiple Savonius Wind Turbines Arrays." (2021). https://doi.org/10.37934/cfdl.12.3.3138

[7] Takey, Mohamed, Tholudin Mat Lazim, Iskandar Shah Ishak, NAR Nik Mohd, and Norazila Othman. "Computational Investigation of a Wind Turbine Shrouded with a Circular Ring." *CFD Letters* 12, no. 10 (2020): 40-51. https://doi.org/10.37934/cfdl.12.10.4051

[8] Wang, X. H., K. H. Wong, W. T. Chong, J. H. Ng, X. B. Xiang, and C. T. Wang. "Experimental investigation of a diffuser-integrated vertical axis wind turbine." In *IOP Conference Series: Earth and Environmental Science*, vol. 463, no. 1, p. 012153. IOP Publishing, 2020. https://doi.org/10.1088/1755-1315/463/1/012153

[9]   Chowdhury, Souma, Jie Zhang, Achille Messac, and Luciano Castillo. "Unrestricted wind farm layout optimization (UWFLO): Investigating key factors influencing the maximum power generation." *Renewable Energy* 38, no. 1 (2012): 16-30. https://doi.org/10.1016/j.renene.2011.06.033

[10]   Segalini, Antonio, and Jan-Åke Dahlberg. "Blockage effects in wind farms." *Wind Energy* 23, no. 2 (2020): 120-128. https://doi.org/10.1002/we.2413

[11]   Zhao, Yi, Ruibin Li, Lu Feng, Yan Wu, Jianlei Niu, and Naiping Gao. "Boundary layer wind tunnel tests of outdoor airflow field around urban buildings: A review of methods and status." *Renewable and Sustainable Energy Reviews* 167 (2022): 112717. https://doi.org/10.1016/j.rser.2022.112717

[12]   Gholamalipour, Payam, Hua Ge, and Ted Stathopoulos. "Wind-driven rain (WDR) loading on building facades: A state-of-the-art review." *Building and Environment* (2022): 109314. https://doi.org/10.1016/j.buildenv.2022.109314

[13]   Hou, Fangwei, and Mohammad Jafari. "Investigation approaches to quantify wind-induced load and response of tall buildings: A review." *Sustainable Cities and Society* 62 (2020): 102376. https://doi.org/10.1016/j.scs.2020.102376

[14]   Bahambary, Khashayar Rahnamay, and Brian Fleck. "A study of inflow parameters on the performance of a wind turbine in an atmospheric boundary layer." *Journal of Advanced Research in Numerical Heat Transfer* 11, no. 1 (2022): 5-11.

[15]   Hang, Wang Xiao, Chong Wen Tong, Wong Kok Hoe, Wang Chin-Tsan, Saw Lip Huat, Poh Sin Chew, and Lai Sai Hin. "Preliminary assessment of optimized accessorial roof shape for performance of wind turbine mounted on eco-roof system." *International Journal of Precision Engineering and Manufacturing-Green Technology* 5 (2018): 375-385. https://doi.org/10.1007/s40684-018-0040-7

[16]   Wang, Xiao Hang, Wen Tong Chong, Kok Hoe Wong, Lip Huat Saw, Sai Hin Lai, Chin-Tsan Wang, and Sin Chew Poh. "The design, simulation and testing of V-shape roof guide vane integrated with an eco-roof system." *Energy Procedia* 105 (2017): 750-763. https://doi.org/10.1016/j.egypro.2017.03.386

[17]   Bardera, Rafael, Ángel Rodríguez-Sevillano, and Adelaida García-Magariño. "Aerodynamic investigation of a morphing wing for micro air vehicle by means of PIV." *Fluids* 5, no. 4 (2020): 191. https://doi.org/10.3390/fluids5040191

[18]   Tabatabaei, Narges, Ramis Örlü, Ricardo Vinuesa, and Philipp Schlatter. "Aerodynamic free-flight conditions in wind tunnel modelling through reduced-order wall inserts." *Fluids* 6, no. 8 (2021): 265. https://doi.org/10.3390/fluids6080265

[19]   Abobaker, Mostafa, Abdulhafid M. Elfaghi, and Sogair Addeep. "Numerical Study of Wind-Tunnel Wall Effects on Lift and Drag Characteristics of NACA 0012 Airfoil." *CFD Letters* 12, no. 11 (2020): 72-82. https://doi.org/10.37934/cfdl.12.11.7282

[20]   Fernández-Gutiérrez, Jana, Pablo Fernández-Arias, Diego Vergara, and Álvaro Antón-Sancho. "An Original Aerodynamic Ducting System to Improve Energy Efficiency in the Automotive Industry." *Inventions* 8, no. 1 (2023): 13. https://doi.org/10.3390/inventions8010013

[21]   Bajuri, Muhammad Nur Arham, Djamal Hissein Didane, Mahamat Issa Boukhari, and Bukhari Manshoor. "Computational Fluid Dynamics (CFD) Analysis of Different Sizes of Savonius Rotor Wind Turbine." *Journal of Advanced Research in Applied Mechanics* 94, no. 1 (2022): 7-12. https://doi.org/10.37934/aram.94.1.712

[22]   Ung, Shern-Khai, Wen-Tong Chong, Shabudin Mat, Jo-Han Ng, Yin-Hui Kok, and Kok-Hoe Wong. "Investigation into the aerodynamic performance of a vertical axis wind turbine with endplate design." *Energies* 15, no. 19 (2022): 6925. https://doi.org/10.3390/en15196925

[23]   Yokoi, Yoshifumi. "Experimental Study of Internal Flow Noise Measurement by Use of a Suction Type Low Noise Wind Tunnel." In *Wind Tunnel Designs and Their Diverse Engineering Applications*. IntechOpen, 2013. https://doi.org/10.5772/53828

[24]   Motin, A., and M. A. T. Ali. "Flow characteristics in the test section of a wind tunnel." In *Proceedings of the 4th BSME-ASME International Conference on Thermal Engineering*. 2014.

[25]   Nader, Gilder, Claudia dos Santos, Paulo JS Jabardo, Monica Cardoso, Nilson M. Taira, and Marcos T. Pereira. "Characterization of low turbulence wind tunnel." In *XVIII IMEKO World Congress-Metrology for a sustainable development*. 2006.

[26]   Quiterio, P. Rosas, M. Toledo Velázquez, G. Tolentino Eslava, R. Tolentino Eslava, and J. Abugaber Francis. "Wind Tunnel at LABINTHAP (Updated)." *Energy and Power Engineering* 3, no. 04 (2011): 565. https://doi.org/10.4236/epe.2011.34070

[27]   Thimmegowda, Hariprasad, and Yadu Krishnan S. "Computational and Experimental Study on Flow Quality of Open-Loop Low-Speed Wind Tunnel." (2021).

[28]   Wang, Lei, Fen Shi, Zheng Wang, and Shuguo Liang. "Blockage Effects in Wind Tunnel Tests for Tall Buildings with Surrounding Buildings." *Applied Sciences* 12, no. 14 (2022): 7087. https://doi.org/10.3390/app12147087

[29] Kaushik, Mrinal. *Theoretical and experimental aerodynamics*. Singapore: Springer, 2019. https://doi.org/10.1007/978-981-13-1678-4

[30] Almeida, Odenir de, Frederico Carnevalli de Miranda, Olivio Ferreira Neto, and Fernanda Guimarães Saad. "Low subsonic wind tunnel-Design and construction." *Journal of Aerospace Technology and Management* 10 (2018). https://doi.org/10.5028/jatm.v10.716

[31] Mauro, Stefano, S. Brusca, R. Lanzafame, F. Famoso, A. Galvagno, and M. Messina. "Small-scale open-circuit wind tunnel: Design criteria, construction and calibration." *International Journal of Applied Engineering Research* 12, no. 23 (2017): 13649-13662.

[32] Santos, J. R., Amarante Mesquita AL RM, and M. L. Gemaque. "Development of an opencircuit low-speed wind tunnel." In *23rd ABCM International Congress of Mechanical Engineering*. 2015.

[33] Eltayesh, Abdelgalil, Magdy Bassily Hanna, Francesco Castellani, A. S. Huzayyin, Hesham M. El-Batsh, Massimiliano Burlando, and Matteo Becchetti. "Effect of wind tunnel blockage on the performance of a horizontal axis wind turbine with different blade number." *Energies* 12, no. 10 (2019): 1988. https://doi.org/10.3390/en12101988

[34] Ross, Ian, and Aaron Altman. "Wind tunnel blockage corrections: Review and application to Savonius vertical-axis wind turbines." *Journal of Wind Engineering and Industrial Aerodynamics* 99, no. 5 (2011): 523-538. https://doi.org/10.1016/j.jweia.2011.02.002

[35] Curd, ERIC F., JORMA RAILIO, JAN GUSTAVSSON, JAAP HOGELING, MAMDOUH EL HAJ ASSAD, JAN EMILSEN, SANTE MAZZACANE, and RALF WIKSTEN. "Air-handling processes." In *Industrial Ventilation Design Guidebook*, pp. 677-806. Academic Press, 2001. https://doi.org/10.1016/B978-012289676-7/50012-6

[36] Teseletso, Atamelang T., Molaletsa Namoshe, N. Subaschandar, and Said Kutua. "Design of an Open-circuit Subsonic Wind Tunnel for Educational Purpose." In *Botswana Institution of Engineers (BIE) 14th International Biennial Conference, At Phakalane, Botswa*. 2015.

[37] Hernández, Miguel A. González, Ana I. Moreno López, Artur A. Jarzabek, José M. Perales Perales, Yuliang Wu, and Sun Xiaoxiao. "Design methodology for a quick and low-cost wind tunnel." *Wind tunnel designs and their diverse engineering applications* 1 (2013): 3-26.

[38] Fluent, A. N. S. Y. S. "R2 User's Manual; ANSYS." *Inc: Canonsburg, PA, USA* (2020).

[39] Pane, Erlanda Augupta, and Reza Abdu Rahman. "An open design for a low-cost open-loop subsonic wind tunnel for aerodynamic measurement and characterization." *HardwareX* 12 (2022): e00352. https://doi.org/10.1016/j.ohx.2022.e00352

[40] Chen, T. Y., and L. R. Liou. "Blockage corrections in wind tunnel tests of small horizontal-axis wind turbines." *Experimental Thermal and Fluid Science* 35, no. 3 (2011): 565-569. https://doi.org/10.1016/j.expthermflusci.2010.12.005